Carrier recombination mechanism at defects in wide band gap two-dimensional materials from first principles

Feng Wu,^{1,*} Tyler J. Smart,^{2,*} Junqing Xu,¹ and Yuan Ping ^{1,†}

¹Department of Chemistry and Biochemistry, University of California Santa Cruz, Santa Cruz, California 95064, USA

²Department of Physics, University of California Santa Cruz, Santa Cruz, California 95064, USA

(Received 5 June 2019; revised manuscript received 20 July 2019; published 19 August 2019)

The identification and design of defects in two-dimensional (2D) materials as promising single photon emitters (SPEs) requires a deep understanding of the underlying carrier recombination mechanisms. Yet, the dominant mechanism of carrier recombination at defects in 2D materials has not been well understood, and some outstanding questions remain: How do recombination processes at defects differ between 2D and 3D systems? What factors determine defects in 2D materials as excellent SPEs at room temperature? In order to address these questions, we developed first-principles methods to accurately calculate the radiative and nonradiative recombination rates at defects in 2D materials, using *h*-BN as a prototypical example. We reveal the carrier recombination mechanism at defects in 2D materials being mostly dominated by defect-defect state recombination in contrast to defect-bulk state recombination in most 3D semiconductors. In particular, we disentangle the nonradiative recombination mechanism into key physical quantities: the zero-phonon line and Huang-Rhys factor. At the end, we identified that strain can effectively tune the electron-phonon coupling at defect centers and drastically change the nonradiative recombination rates. Our theoretical development serves as a general platform for understanding carrier recombination at defects in 2D materials, while providing pathways for engineering of quantum efficiency of SPEs.

DOI: 10.1103/PhysRevB.100.081407

The engineering of spin defects in wide band semiconductors offers a promising avenue for the development of quantum spin devices [1–4]. They are among the few alternatives for quantum technologies that operate at room temperature. Deep defects in two-dimensional (2D) materials such as hexagonal boron nitride (h-BN) [5–17] and transition-metal dichalcogenides (TMDs) [18,19] have proven to be promising single photon sources with polarized and ultrabright single photon emission at room temperature. These materials exhibit an unprecedented potential for several applications, including large-scale nanophotonics and quantum information processing [20–24], which in turn provide a new platform for exploring quantum phenomena [4]. In order for these defect centers to provide bright single photon emitters (SPEs) [1,23], the radiative recombination rate (photon emitted) needs to be high, while the nonradiative recombination rate (no photon emitted) must be substantially lower to yield a high quantum efficiency. Furthermore, a weak electron-phonon coupling is also required to ensure a long spin relaxation time for the application of qubit and stable single photon emission at room temperature.

Despite the importance of maximizing radiative rates for quantum information, the factors which determine the recombination process at defects in 2D materials are not understood experimentally or theoretically. Past theoretical studies have either focused on radiative recombination in pristine 2D materials [25–27] or phonon-assisted nonradiative recombination

for defects in 3D wide band gap semiconductors [28,29]. Therefore, a fully comparative study of both recombination processes for defect centers in 2D materials is highly desired.

Furthermore, the high tunability of SPEs allows them to be integrated within a vast array of applications [6,23]. Among these methods, strain modulation is one of the most effective strategies, especially for low-dimensional materials which can work under large distortion [30]. For example, in 2D systems, some key electronic properties, such as the band gap, change by 1.5% under 1% uniaxial tension in TMD monolayers [31] or 6% under 1% uniaxial tension in phosphorene [32]. Additionally, the nonradiative process, which is intrinsically sensitive to lattice deformation (as it is phonon mediated), may exhibit even more drastic changes under strain.

In this Rapid Communication, we first introduce the formalism of computing the radiative and nonradiative lifetimes of defect excited states from first principles. We then focus on comparing the radiative and nonradiative processes of different transitions in a series of important defects in monolayer h-BN, where we discuss the dominant recombination processes and their implication on SPE efficiency. Finally, we show that applying strain to h-BN defects can effectively tune the nonradiative rates and quantum yield of SPEs.

The radiative and nonradiative transition rates between two electronic states under perturbation can be computed via Fermi's golden rule,

$$r_{if}^{R} = \frac{2\pi}{\hbar} g |\langle f|H^{R}|i\rangle|^{2} \delta(E_{i} - E_{f}), \tag{1}$$

$$r_{if}^{NR} = \frac{2\pi}{\hbar} g \sum_{n,m} p_{\rm in} |\langle fm| H^{e\text{-ph}} |in\rangle|^2 \delta(E_{\rm in} - E_{fm}). \quad (2)$$

^{*}These authors contributed equally to this work.

[†]yuanping@ucsc.edu

Here, r_{if}^R and r_{if}^{NR} denote the recombination rates between electronic states i and f via a radiative process (r_{if}^R) and nonradiative process (r_{if}^{NR}) , respectively. g is the degeneracy factor of the final state, i.e., several equivalent energy-degenerate atomic configurations of the final state might exist [33]. For defects in 2D materials studied in this work, g factors are all equal to 1. H^R is the electron-photon coupling (electromagnetic) Hamiltonian and H^{e-ph} is the electron-phonon coupling Hamiltonian. A sum over phonon states n, m enters the nonradiative recombination process with an occupation number $p_{\rm in}$ of the vibronic state $|in\rangle$. For ground-state calculations, we employed the open source plane-wave code QUANTUM ESPRESSO [34] with optimized norm-conserving Vanderbilt (ONCV) pseudopotentials [35,36] and a supercell size of 6 × 6 or higher. Charge corrections for the total energies and eigenvalues of charged defects were applied by employing the techniques developed in Refs. [26,37]. The total energies, defect formation energies, and geometry were computed at both Perdew-Burke-Ernzerhof (PBE) and hybrid functional levels [the results presented in the main text are computed at PBE, and a detailed comparison between the two levels can be found in the Supplemental Material (SM) Table S4 [38]]. The band gaps of pristine h-BN are computed at GW@PBE as done in our previous work [26], which are 6.01 eV for bulk and 7.01 eV for monolayer h-BN, respectively. The exciton dipole moments and exciton energies as input for the radiative lifetime were computed at many-body perturbation theory with the GW approximation for quasiparticle energies [39–41] and then solving the Bethe-Salpeter equation with the YAMBO code [42], as well as the random phase approximation (RPA) with density functional theory (DFT) eigenvalues (a detailed comparison can be found in the SM. Table S3: the results in the main text are computed at DFT-RPA). More computational details and formulation of radiative rates r_{if}^{R} are discussed in the SM and Ref. [43].

The nonradiative rate is simplified by the static coupling approximation with a one-dimensional (1D) effective phonon approximation [28–30,33,44–57] [the validation of the 1D effective phonon approximation in h-BN is based on the similarity of Huang-Rhys (HR) factors between the 1D effective phonon and all phonon calculations, as discussed in the SM, Sec. IV],

$$r_{if}^{NR} = \frac{2\pi}{\hbar} g|W_{if}|^2 X_{if}(T), \qquad (3)$$

$$X_{if}(T) = \sum_{n,m} p_{\text{in}} |\langle \phi_{fm}(\mathbf{R}) | Q - Q_a | \phi_{\text{in}}(\mathbf{R}) \rangle|^2$$

$$\times \delta(m\hbar\omega_f - n\hbar\omega_i + \Delta E_{if}), \tag{4}$$

$$W_{if} = \langle \psi_i(\mathbf{r}, \mathbf{R}) | \frac{\partial H}{\partial O} | \psi_f(\mathbf{r}, \mathbf{R}) \rangle |_{\mathbf{R} = \mathbf{R}_a}, \tag{5}$$

where r_{if}^{NR} is naturally separated into an electronic term W_{if} and a phonon term $X_{if}(T)$ with the temperature dependence from the thermal population $(p_{\rm in})$. Here, ΔE_{if} is the zerophonon line energy (ZPL), which can be measured experimentally by photoluminescence. We implemented the nonradiative recombination rates as postprocessing codes of QUANTUM ESPRESSO [34].

TABLE I. Nonradiative lifetimes and capture coefficients of defects in h-BN and GaN through defect-band recombination (only for the hole capture processes $A^{-1} + h^+ \rightarrow A^0$). For comparison, a dominant defect-defect recombination at $N_B V_N$ in monolayer h-BN is also listed. The capture coefficients C_p (with a unit of cm²/s for 2D and cm³/s for 3D systems) and lifetimes are reported at T = 300 K. Lifetimes are defined as the inverse of rates $\tau^{NR} = 1/r_{if}^{NR}$ and computed in a 6 × 6 h-BN supercell or 2 × 2 × 2 GaN supercell.

System	ZPL (eV)	ΔQ (amu ^{1/2} Å)	$\hbar\omega_f$ (meV)	C_p (cm ⁿ /s)	$ au^{NR}$
$\overline{ML C_B V_N (2D)}$	5.78	0.58	86	10^{-32}	>1 ms
$ML O_B O_B V_N (2D)$	4.26	0.84	85	10^{-29}	>1 ms
$ML N_B V_N (2D)$	5.46	0.51	95	10^{-33}	>1 ms
$ML C_N (2D)$	3.87	0.35	150	10^{-16}	>1 ms
Bulk C_N (3D)	2.69	0.35	149	10^{-16}	$6.6 \mu s$
$GaN-C_N$ (3D)	1.00	1.39	39	10^{-9} a	0.29 ps
ML $N_B V_N$ (2D) (defect-defect)	2.04	0.53	100	10^{-4}	102 ps

 $^{^{}a}7 \times 10^{-10}$ in Ref. [33].

A single defect may introduce several energy levels within the band gap of the host material. This yields the possibility for transitions to occur between defect states ("defect-defect" transition), as well as from a defect state to a band edge ("defect-band" transition). The computed nonradiative lifetimes and capture coefficients of the most probable defectband transitions for hole captures in multiple defects in monolayer and bulk h-BN as well as bulk GaN are listed in Table I [where X_BV_N (X = C, O, N) denotes X substitution of boron accompanied by a nitrogen vacancy]. The capture coefficients are defined as a product of recombination rates r_{ij} with the surface area or volume for 2D or 3D systems, respectively. The corresponding defect formation energies and configuration coordinate diagrams are presented in the SM, Fig. S1. We find that all defect-band transitions in monolayer h-BN have very small rates (the corresponding lifetime exceeds milliseconds). This is in contrast to typical 3D bulk defects in other materials, such as $GaN-C_N$ or $GaN-(Zn_{Ga}V_N)$, where the nonradiative lifetime is at the picosecond level with a similar defect concentration to h-BN [33,53,58].

One key reason that nonradiative defect-band recombination in monolayer h-BN is typically slow, is due to large energy differences between the defect states and band edges $(\sim 4-6 \text{ eV})$ as the ZPL shown in Table I [26,59,60]. Nonetheless, other factors such as the effective phonon frequencies $\hbar\omega_f$ and the change of nuclear positions ΔQ can also affect the rates, as discussed later. For example, comparing monolayer BN-C_N with bulk BN-C_N, only the ZPL changes significantly (over 1 eV) and other parameters ($\hbar\omega_f$ and ΔQ) remain nearly constant, which ultimately leads to a two order of magnitude difference in their capture rates. Physically, the phonon-assisted nonradiative rate is dominated by a charge transfer process between the initial and final state potential energy surfaces, and can be approximated by a classical Marcus' theory picture (see Fig. 1). Given the form of the energy barrier for charge transfer [30], a large energy difference between the two states (ZPL) results in an exponential drop in the transfer rate (although exceptions can be found [29,61–63]).

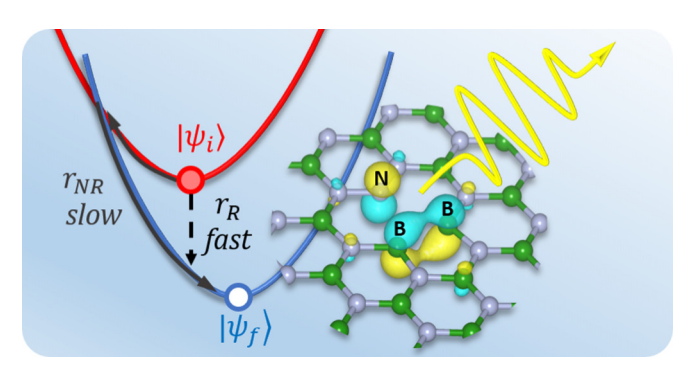


FIG. 1. Schematic diagram of carrier recombination at the N_BV_N defect in monolayer h-BN. In order for a defect to be a robust single photon source, it is necessary for the radiative recombination rates to be much higher than the nonradiative ones.

Therefore, in monolayer h-BN, the large ZPLs of defect-band transitions result in extremely slow nonradiative recombination processes (over milliseconds). On the other hand, several defects have allowed defect-defect transitions with viable nonradiative rates due to smaller energy differences, e.g., the N_BV_N (nitrogen substitution of boron accompanied by a nitrogen vacancy) defect-defect transition in monolayer h-BN (Table II).

Hence, the remaining discussions are focused on defect-defect transitions in monolayer *h*-BN. Defect-defect nonradiative recombination is performed for neutral excited and ground states with a constrained occupation number. The equilibrium geometry, ZPL, and vibrational frequency can be also obtained at DFT with a constrained occupation. More computational details for defect-defect nonradiative recombination can be found in SM, Sec. III, Fig. S2, and Table S4.

Considering a typical point defect such as N_BV_N which has been proposed as a promising defect for SPE [6,12,64], we find it introduces several isolated energy levels that lead to multiple possible radiative and nonradiative defect-defect recombination pathways (as shown in Fig. 2). However, we found only the transition between $1B_1 \uparrow$ and $2B_1 \uparrow$ [highest occupied molecular orbital(HOMO)-lowest unoccupied molecular orbital (LUMO) transition for the majority spin channel] has a viably short radiative lifetime and nonradiative lifetime. All other processes have a nonradiative lifetime longer than ms, much slower than this transition which is at a picosecond level.

TABLE II. Properties of defect-defect nonradiative recombination of the N_BV_N defect in monolayer h-BN. Nonradiative lifetimes are computed with a 6×6 supercell at 300 K and S_f denotes the ground-state Huang-Rhys factor.

Transition		$\hbar\omega_f$ (meV)	k ^a	S_f	X_{if}	W_{if}	$\frac{C_p}{(\text{cm}^2/\text{s})}$	$ au^{NR}$ (ps)
$2B_1\uparrow/1B_1\uparrow$	2.04	100	20	5.3	1.3	0.38	10^{-4}	102
$1B_1\downarrow/1A_1\downarrow$	1.33							$> 10^9$
$2B_1\downarrow/1A_1\downarrow$	2.94	65	46	7.8	10^{-4}	10^{-6}	10^{-19}	$> 10^9$
$2B_1{\downarrow}/1B_1{\downarrow}$	1.61	57	28	3.2	10^{-13}	0.03	10^{-19}	$> 10^9$

 $^{^{}a}k = \Delta E_{if}/\hbar\omega_{f}$.

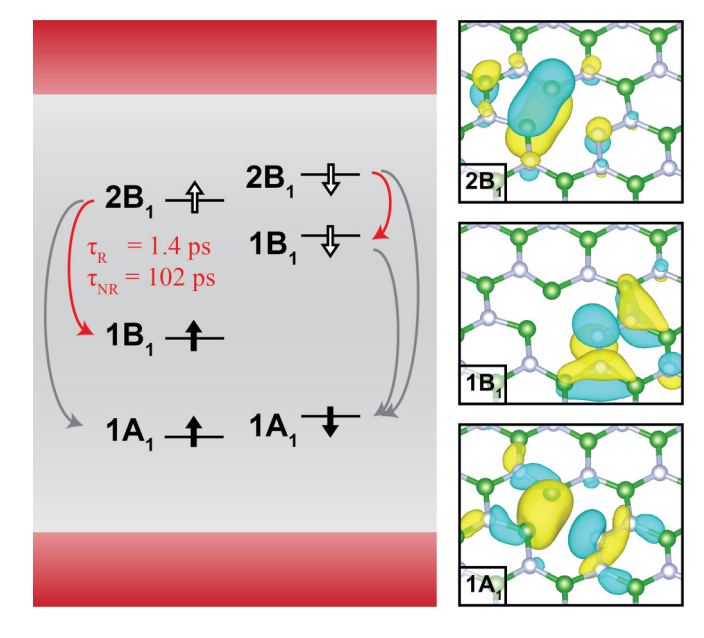


FIG. 2. Defect levels and possible defect-defect transitions of N_BV_N in monolayer h-BN. Both up and down spin channels of the $2B_1/1B_1$ transitions are marked in red as they are optically allowed with light polarized along defect C_2 symmetry axis. The exact radiative (τ_R) and nonradiative (τ_{NR}) lifetimes are given for the spin-up transition with a 6×6 supercell. The remaining transitions in gray are all optically forbidden and have very long radiative and nonradiative recombination lifetimes (exceeding 1 ms).

The nonradiative transition rate is determined by multiple factors based on Eq. (3). The first factor is the phonon term X_{if} . As the ZPL for all defect-defect transitions are relatively small (less than 3 eV, unlike defect-band transitions), we analyze the subtle difference causing the variation of X_{if} among different transitions, based on the relation $X_{if} \propto e^{-S\frac{\hat{S}^k}{k!}}$, where $k \approx \Delta E_{if}/\hbar\omega_f$ and S is the HR factor [33]. Specifically (k > S)for all defect-defect transitions we study here), a high S implies a large electron-phonon coupling and generally will increase the phonon contribution X_{if} . For example, the HR factor for the $1B_1\downarrow/1A_1\downarrow$ transition (16.6) is several times larger than other transitions in Table II and therefore yields the largest X_{if} of 10^5 at 300 K. On the other hand, a high value of k means a large energy difference (ZPL) relative to the phonon frequency and will reduce the phonon contribution X_{if} , similar to earlier discussions on defect-band transitions. The second factor is the electronic term W_{if} , which is proportional to the overlap between electronic wave functions $\langle \psi_i | \psi_f \rangle$. Ultimately, only the $2B_1 \uparrow / 1B_1 \uparrow$ transition has a reasonably large X_{if} and the largest W_{if} , which leads to a viable nonradiative recombination process with a lifetime of 102 ps

TABLE III. Properties of the $1B_1 \uparrow -2B_1 \uparrow$ defect-defect state transition for the $N_B V_N$ defect in monolayer h-BN under strain. Strain directions are shown in Fig. 3. X_{if} and lifetime are reported at 300 K.

Strain	ZPL (eV)	ΔQ (Å)	$\hbar\omega_f$ (meV)	S_f	W_{if}	X_{if}	τ^{NR} (ps)
No strain	2.04	0.666	100	5.33	0.38	1.26	102
Biaxial −1%	2.08	0.613	105	4.69	0.39	0.28	429
Biaxial 1%	2.01	0.732	96	6.18	0.36	9.20	16
Uniaxial ∥ −1%	2.02	0.637	102	4.96	0.39	0.95	127
Uniaxial 1%	2.07	0.703	98	5.80	0.36	1.98	70
Uniaxial $\perp -1\%$	2.10	0.642	103	5.05	0.38	0.38	336
Uniaxial ⊥1%	1.98	0.697	98	5.69	0.37	5.39	25

in short radiative lifetimes of 1.4 and 2.5 ps, respectively. This lifetime can be considered to be a lower bound compared to that of experimental results, because a much higher defect concentration is adopted in practical calculations (one defect in a 72-atom supercell, i.e., one defect per 2 nm², compared to the order of one SPE per μ m² in experiments [6]) and both radiative and nonradiative lifetimes will increase linearly with decreasing defect concentrations or increasing supercell size (see Ref. [46] and Sec. V, Tables S1 and S2 in the SM). At the low concentration limit, we can consider the defect acts as an isolated molecule in the 2D plane [43], which gives an upper bound of the actual lifetime, i.e., 40 ns for $2B_1 \uparrow / 1B_1 \uparrow$ radiative lifetime at N_BV_N. This is in good agreement with the experimental radiative lifetimes of monolayer h-BN SPEs, which are measured to be on the order of ns [6,8,9,11]. We note that different from the recombination rates, the capture coefficient is generally constant as a function of defect concentration or supercell sizes (see Tables S1 and S2 in

The quantum yield of a SPE (excluding substrate effects) is defined as $\gamma_{if} = r_{if}^R/(r_{if}^R + r_{if}^{NR})$ [65–67]. By comparing the radiative lifetimes with the nonradiative ones shown in Table II for the N_BV_N defect, we have $\gamma > 98\%$, which shows it has the potential to be a highly efficient quantum emitter. In practice, several other external effects can cause the quantum yield to be substantially lower. In particular, substrate recombination [68], photobleaching [69], and strain (discussed in the next section) are known to play the role of limiting the quantum yield of defect SPEs.

In this Rapid Communication, we discuss the impact of strain on nonradiative recombination (and leave other external effects for future study) with $N_B V_N$ as an example. Presumably, strain will change the radiative lifetime little (orbital overlaps between initial and final states are largely preserved) compared to that of the nonradiative lifetime which can be strongly affected by changes in local structures. As shown in Fig. 3, strain may be applied along the C_2 symmetry axis (denoted as \parallel strain) or orthogonal to the symmetry axis (denoted as \perp strain). We consider effects of strain along both directions as well as the combinatory effects of biaxial strain for the $2B_1 \uparrow /1B_1 \uparrow$ transition (shown in Table III).

As discussed earlier, the nonradiative recombination rate is composed of an electronic term W_{if} and a phonon term X_{if} . Because W_{if} is proportional to the wave-function overlap,

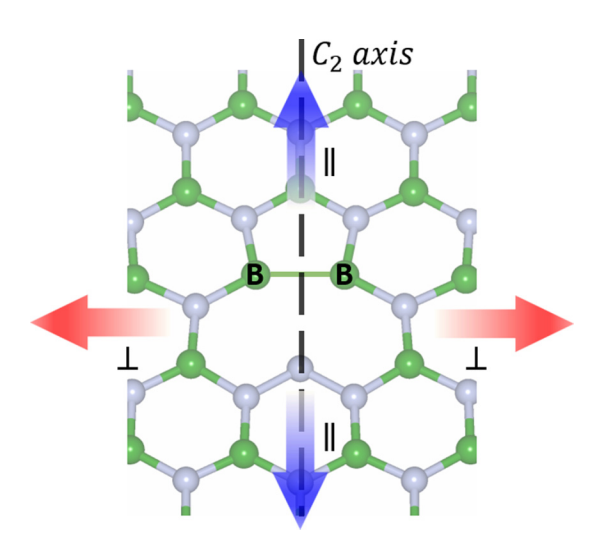


FIG. 3. Illustration of the directions of uniaxial strain based on the C_{2v} symmetry of N_BV_N in h-BN. Uniaxial strains applied parallel (\parallel blue arrows) or perpendicular (\perp red arrows) to the C_2 axis are considered. The optimized atomic structure of N_BV_N defect is also shown. The green balls denote B atoms and the gray balls denote N atoms.

the change in W_{if} due to strain is found to be negligible, as shown in Fig. 4(a). However, there are significant changes of the phonon term X_{if} due to strain. We note that compressive strain indicates lattice shrinking (-), while tensile strain indicates lattice stretching (+) and induces opposite changes on nonradiative rates from the former. Therefore, we only discuss compressive strain here. First, compressive strain decreased interatomic distances, which in turn decreased the change in the atomic coordination between the initial and final states $(\Delta Q \text{ in Table III})$. As such, under compressive strain, the HR factor $S = \omega_f \Delta Q^2 / 2\hbar$ decreased, resulting in an exponential decrease of the phonon term X_{if} . Such trends occurred regardless of the direction of strain applied (i.e., \perp or \parallel to the C_2 axis). Second, a change in the ZPL also occurred under strain [9]. After the formation of the nitrogen vacancy, a weak B-B bond is formed perpendicular to the C_2 symmetric axis (see Fig. 3). When compressive strain is applied perpendicular to the C_2 axis (\perp strain), the ZPL is increased, due to larger bonding-antibonding splitting of the B-B bond that shifts up the 2B₁ energy level (see Fig. 2 for related wave functions and energy levels). As a result, for \perp strain the change in ZPL and HR factor coincided and yielded an exponential decrease of X_{if} under compressive strain [red curve, Fig. 4(b)]. In contrast, for || strain, these changes counteracted each other, resulting in a nearly constant value of X_{if} [blue curve, Fig. 4(b)]. In addition, biaxial strain is a simple combinatory effect of || and \perp strain, mostly dominated by the trend of \perp strain [black curve, Fig. 4(b)]. All in all, the exponential change in X_{if} for both biaxial and uniaxial \perp strain resulted in an exponential modification to the nonradiative lifetime of the defect, as black and red curves shown in Fig. 4(c). In particular, in the case of tensile biaxial strain, with 1%, the quantum yield decreased by 10% due to an order of magnitude decrease in nonradiative lifetime. This highlights the significant impact strain can have on the efficiency of defect SPE.

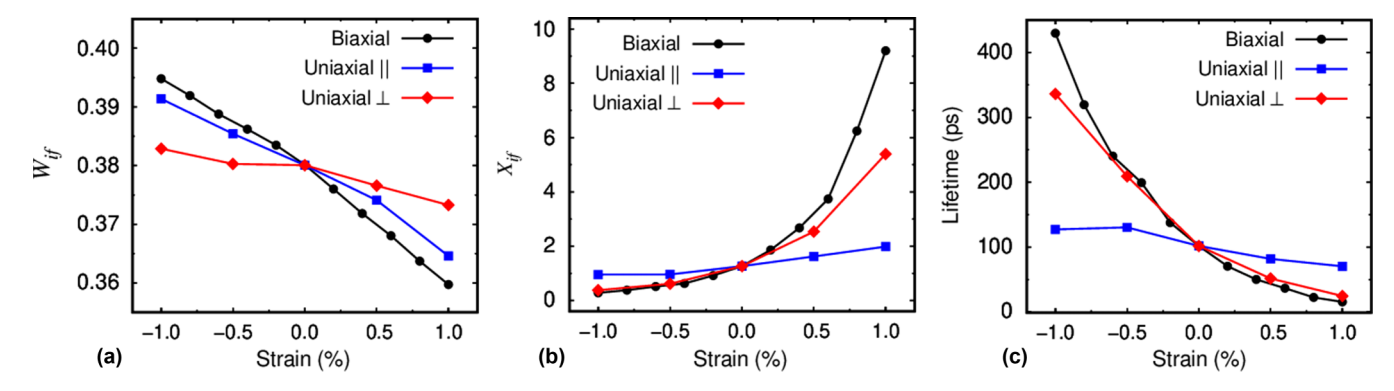


FIG. 4. Strain-induced properties related to the nonradiative recombination lifetime of the $1B_1-2B_1$ defect-defect transition of N_BV_N in monolayer h-BN. Strain directions are shown in Fig. 3.

In summary, in this Rapid Communication we compared the radiative and phonon-assisted nonradiative recombinations at defects in wide band gap 2D materials, using monolayer h-BN as a prototypical example. We found the radiative recombination rates far surpass the nonradiative ones, highlighting the potential of point defects in wide band gap 2D materials as single photon emitters. Defect-band nonradiative recombinations all have negligible rates possibly due to large energy differences between the initial and final states, and only a small subset of defect-defect nonradiative transitions are possible. Transitions vary on several orders of magnitude due to wave-function symmetry, HR factor, as well as the zero-phonon line (ZPL). Finally, we show that compressive or tensile strain up to 1% can alter the nonradiative lifetime by orders of magnitude. Hence, strain largely impacts the quantum yield of single photon emitters and alters the photon energy of the emitter for use towards specific optoelectronic applications. Our study provides important insights on the critical factors of defects in 2D materials as single photon emitters for quantum information applications.

We acknowledge L.-W. Wang, A. Alkauskas, and C. Dreyer for helpful discussions. This work is supported by National Science Foundation under Grants No. DMR-1760260 and No. DMR-1747426, and the Hellman Fellowship. This research used resources of the Center for Functional Nanomaterials, which is a U.S. DOE Office of Science Facility, and the Scientific Data and Computing center, a component of the Computational Science Initiative, at Brookhaven National Laboratory under Contract No. DE-SC0012704, the National Energy Research Scientific Computing Center (NERSC) a U.S. Department of Energy Office of Science User Facility operated under Contract No. DE-AC02-05CH11231, and the Extreme Science and Engineering Discovery Environment (XSEDE) which is supported by National Science Foundation Grant No. ACI-1548562 [70].

I. Aharonovich, S. Castelletto, D. A. Simpson, C.-H. Su, A. D. Greentree, and S. Prawer, Rep. Prog. Phys. 74, 076501 (2011).

^[2] T. D. Ladd, F. Jelezko, R. Laflamme, Y. Nakamura, C. Monroe, and J. L. O'Brien, Nature (London) 464, 45 (2010).

^[3] H. Seo, M. Govoni, and G. Galli, Sci. Rep. 6, 20803 (2016).

^[4] C. E. Dreyer, A. Alkauskas, J. L. Lyons, A. Janotti, and C. G. Van de Walle, Annu. Rev. Mater. Res. 48, 1 (2018).

^[5] I. Aharonovich and E. Neu, Adv. Opt. Mater. 2, 911 (2014).

^[6] T. T. Tran, K. Bray, M. J. Ford, M. Toth, and I. Aharonovich, Nat. Nanotechnol. 11, 37 (2016).

^[7] S. Kim, J. E. Fröch, J. Christian, M. Straw, J. Bishop, D. Totonjian, K. Watanabe, T. Taniguchi, M. Toth, and I. Aharonovich, Nat. Commun. 9, 2623 (2018).

^[8] R. Bourrellier, S. Meuret, A. Tararan, O. Stéphan, M. Kociak, L. H. G. Tizei, and A. Zobelli, Nano Lett. 16, 4317 (2016).

^[9] G. Grosso, H. Moon, B. Lienhard, S. Ali, D. K. Efetov, M. M. Furchi, P. Jarillo-Herrero, M. J. Ford, I. Aharonovich, and D. Englund, Nat. Commun. 8, 705 (2017).

^[10] X. Li, G. D. Shepard, A. Cupo, N. Camporeale, K. Shayan, Y. Luo, V. Meunier, and S. Strauf, ACS Nano 11, 6652 (2017).

^[11] A. L. Exarhos, D. A. Hopper, R. R. Grote, A. Alkauskas, and L. C. Bassett, ACS Nano 11, 3328 (2017).

^[12] A. L. Exarhos, D. A. Hopper, R. N. Patel, M. W. Doherty, and L. C. Bassett, Nat. Commun. 10, 222 (2019).

^[13] L. Museur, E. Feldbach, and A. Kanaev, Phys. Rev. B 78, 155204 (2008).

^[14] B. Sontheimer, M. Braun, N. Nikolay, N. Sadzak, I. Aharonovich, and O. Benson, Phys. Rev. B 96, 121202(R) (2017).

^[15] N. R. Jungwirth, B. Calderon, Y. Ji, M. G. Spencer, M. E. Flatté, and G. D. Fuchs, Nano Lett. 16, 6052 (2016).

^[16] N. R. Jungwirth and G. D. Fuchs, Phys. Rev. Lett. 119, 057401 (2017).

^[17] G. Noh, D. Choi, J.-H. Kim, D.-G. Im, Y.-H. Kim, H. Seo, and J. Lee, Nano Lett. 18, 4710 (2018).

^[18] K. F. Mak and J. Shan, Nat. Photonics 10, 216 (2016).

^[19] C. Palacios-Berraquero, D. M. Kara, A. R.-P. Montblanch, M. Barbone, P. Latawiec, D. Yoon, A. K. Ott, M. Loncar, A. C. Ferrari, and M. Atatüre, Nat. Commun. 8, 15093 (2017).

^[20] A. Beveratos, R. Brouri, T. Gacoin, A. Villing, J.-P. Poizat, and P. Grangier, Phys. Rev. Lett. 89, 187901 (2002).

^[21] J. L. O'Brien, A. Furusawa, and J. Vučković, Nat. Photonics 3, 687 (2009).

- [22] V. Scarani, H. Bechmann-Pasquinucci, N. J. Cerf, M. Dušek, N. Lütkenhaus, and M. Peev, Rev. Mod. Phys. 81, 1301 (2009).
- [23] I. Aharonovich, D. Englund, and M. Toth, Nat. Photonics 10, 631 (2016).
- [24] T. Vogl, G. Campbell, B. C. Buchler, Y. Lu, and P. K. Lam, ACS Photonics 5, 2305 (2018).
- [25] M. Palummo, M. Bernardi, and J. C. Grossman, Nano Lett. 15, 2794 (2015).
- [26] F. Wu, A. Galatas, R. Sundararaman, D. Rocca, and Y. Ping, Phys. Rev. Mater. 1, 071001 (2017).
- [27] H.-Y. Chen, M. Palummo, D. Sangalli, and M. Bernadi, Nano Lett. 18, 3839 (2018).
- [28] A. Alkauskas, B. B. Buckley, D. D. Awschalom, and C. G. V. de Walle, New J. Phys. 16, 073026 (2014).
- [29] L. Shi, K. Xu, and L.-W. Wang, Phys. Rev. B 91, 205315 (2015).
- [30] N. P. Brawand, M. Vörös, and G. Galli, Nanoscale 7, 3737 (2015).
- [31] C.-H. Chang, X. Fan, S.-H. Lin, and J.-L. Kuo, Phys. Rev. B 88, 195420 (2013).
- [32] X. Peng, Q. Wei, and A. Copple, Phys. Rev. B 90, 085402 (2014).
- [33] A. Alkauskas, Q. Yan, and C. G. Van de Walle, Phys. Rev. B 90, 075202 (2014).
- [34] P. Giannozzi, S. Baroni, N. Bonini, M. Calandra, R. Car, C. Cavazzoni, D. Ceresoli, G. L. Chiarotti, M. Cococcioni, I. Dabo et al., J. Phys.: Condens. Matter 21, 395502 (2009).
- [35] D. R. Hamann, Phys. Rev. B 88, 085117 (2013).
- [36] M. Schlipf and F. Gygi, Comput. Phys. Commun. 196, 36 (2015).
- [37] R. Sundararaman and Y. Ping, J. Chem. Phys. 146, 104109 (2017).
- [38] See Supplemental Material at http://link.aps.org/supplemental/ 10.1103/PhysRevB.100.081407 for computational details, description of methods to compute radiative and nonradiative lifetime, defect formation energies, charge transition levels and configuration diagrams of defect-defect transitions in h-BN, convergence of supercell sizes, and results from different levels of theory and DFT exchange-correlation functionals.
- [39] M. Govoni and G. Galli, J. Chem. Theory Comput. 11, 2680 (2015).
- [40] Y. Ping, D. Rocca, and G. Galli, Chem. Soc. Rev. 42, 2437 (2013).
- [41] H.-V. Nguyen, T. A. Pham, D. Rocca, and G. Galli, Phys. Rev. B 85, 081101(R) (2012).
- [42] A. Marini, C. Hogan, M. Grüning, and D. Varsano, Comput. Phys. Commun. **180**, 1392 (2009).
- [43] F. Wu, D. Rocca, and Y. Ping, J. Mater. Chem. C, doi:10.1039/C9TC02214G (2019).
- [44] G. D. Barmparis, Y. S. Puzyrev, X.-G. Zhang, and S. T. Pantelides, Phys. Rev. B **92**, 214111 (2015).

- [45] A. Alkauskas, J. L. Lyons, D. Steiauf, and C. G. Van de Walle, Phys. Rev. Lett. 109, 267401 (2012).
- [46] A. Alkauskas, M. D. McCluskey, and C. G. Van de Walle, J. Appl. Phys. 119, 181101 (2016).
- [47] F. Giustino, Rev. Mod. Phys. 89, 015003 (2017).
- [48] C. H. Henry and D. V. Lang, Phys. Rev. B 15, 989 (1977).
- [49] D. W. Howgate, Phys. Rev. 177, 1358 (1969).
- [50] B. Monserrat, J. Phys.: Condens. Matter **30**, 083001 (2018).
- [51] R. Pässler, Czech. J. Phys. B 24, 322 (1974).
- [52] R. Pässler, Phys. Status Solidi B 78, 625 (1976).
- [53] L. Shi and L.-W. Wang, Phys. Rev. Lett. 109, 245501 (2012).
- [54] D. Wickramaratne, J.-X. Shen, A. Alkauskas, and C. G. Van de Walle, Phys. Rev. B 97, 077301 (2018).
- [55] L. Shi, K. Xu, and L.-W. Wang, Phys. Rev. B 97, 077302 (2018).
- [56] J.-H. Yang, L. Shi, L.-W. Wang, and S.-H. Wei, Sci. Rep. 6, 21712 (2016).
- [57] A. M. Stoneham, Theory of Defects in Solids: Electronic Structure of Defects in Insulators and Semiconductors (Oxford University Press, Oxford, U.K., 2001).
- [58] M. A. Reshchikov, in *International Conference on Defects in Semiconductors: Proceedings of the 27th International Conference on Defects in Semiconductors, ICDS-2013*, edited by A. Cavallini and S. K. Estreicher, AIP Conf. Proc. 1583 (AIP, Melville, NY, 2014), p. 127.
- [59] T. J. Smart, F. Wu, M. Govoni, and Y. Ping, Phys. Rev. Mater. 2, 124002 (2018).
- [60] F. A. Rasmussen, P. S. Schmidt, K. T. Winther, and K. S. Thygesen, Phys. Rev. B 94, 155406 (2016).
- [61] G. Nan, X. Yang, L. Wang, Z. Shuai, and Y. Zhao, Phys. Rev. B 79, 115203 (2009).
- [62] J. Jortner, J. Chem. Phys. 64, 4860 (1976).
- [63] R. Pässler, Czech. J. Phys. B 32, 846 (1982).
- [64] M. Abdi, J.-P. Chou, A. Gali, and M. B. Plenio, ACS Photonics 5, 1967 (2018).
- [65] J. I. Pankove, Optical Processes in Semiconductors (Courier Corporation, North Chelmsford, MA, 1975).
- [66] T. Chevallier, A. Benayad, G. Le Blevennec, and F. Chandezon, Phys. Chem. Chem. Phys. 19, 2359 (2017).
- [67] Y. Hamanaka, K. Ozawa, and T. Kuzuya, J. Phys. Chem. C 118, 14562 (2014).
- [68] M. R. Rosenberger, H.-J. Chuang, K. M. McCreary, C. H. Li, and B. T. Jonker, ACS Nano 12, 1793 (2018).
- [69] L. J. Martínez, T. Pelini, V. Waselowski, J. Maze, B. Gil, G. Cassabois, and V. Jacques, Phys. Rev. B 94, 121405(R) (2016).
- [70] J. Towns, T. Cockerill, M. Dahan, I. Foster, K. Gaither, A. Grimshaw, V. Hazlewood, S. Lathrop, D. Lifka, G. D. Peterson et al., Comput. Sci. Eng. 16, 62 (2014).